Journal of Alloys and Compounds 784 (2019) 1047–1061

Contents lists available at ScienceDirect

Journal of Alloys and Compounds

journal homepage: http://www.elsevier.com/locate/jalcom

Production of aluminum alloy-based metal matrix composites using scrap aluminum alloy and waste materials: Influence on microstructure and mechanical properties

Pradeep Kumar Krishnan [a], John Victor Christy [b], Ramanathan Arunachalam [c, *], Abdel-Hamid I. Mourad [b], Rajaraman Muraliraja [d], Majid Al-Maharbi [c], Venkatraman Murali [a], Majumder Manik Chandra [e]

[a] National University of Science and Technology, Oman
[b] United Arab Emirates University, Al-Ain, United Arab Emirates
[c] Sultan Qaboos University, Oman
[d] Vels Institute of Science, Technology & Advanced Studies (VISTAS), India
[e] National Institute of Technology, Durgapur, India

ARTICLE INFO

Article history:
Received 20 November 2018
Received in revised form
8 January 2019
Accepted 10 January 2019
Available online 11 January 2019

Keywords:
Aluminium metal matrix composites
Scrap aluminium alloy wheels
Spent alumina catalyst
Squeeze casting
Hardness
Mechanical properties

ABSTRACT

In the present study, aluminium metal matrix composites (AMCs) were successfully produced through stir-squeeze casting using a novel approach. The feasibility of using car scrap aluminium alloy wheels (SAAWs) as the matrix material and spent alumina catalyst (SAC) from oil refineries as reinforcement material was investigated. For the purpose of comparision, composites were also produced using AlSi7Mg (LM25 grade) aluminium alloy as a matrix and alumina as reinforcement particles through the stir-squeeze casting process. In total, four different combinations of composites (AlSi7Mg + alumina; scrap aluminium alloy + alumina; AlSi7Mg + spent alumina catalyst; scrap aluminium alloy + spent alumina catalyst) were produced and characterized. Microstructural investigations using an optical microscope and a scanning electron microscope (SEM) as well as energy dispersive X-ray spectroscopy (EDS) and X-ray diffraction (XRD) revealed that in all four composites the reinforcement formed a mixture in the eutectic silicon phase of the matrix alloy. The alumina particles' size and content ratio greatly influenced this mixture's formation and morphology. The composites produced using alumina exhibited smaller pore sizes and lower porosity as compared to the composites produced with a spent alumina catalyst. Superior mechanical properties were also obtained when using alumina as reinforcement, and better mechanical properties can mainly be attributed to the morphology of the reinforcement and silicon eutectic phase mixture. The scrap aluminium alloy + alumina exhibited the lowest porosity (7.3%) and abrasive wear loss (0.11 mg for the finest abrasive), highest hardness (58.5 BHN), and second highest ultimate tensile strength (UTS) (125 MPa) and ultimate compressive strength (UCS) (312 MPa) among the four composites.

1. Introduction

Aluminum is widely available in the Earth's crust and accounts for about 8% by weight of the Earth's stable surface. Its properties, such as high strength-to-weight ratio, ductility, durability, etc., and abundant availability have attracted researchers and caused industries to prefer it. For these reasons, global aluminum demand has increased [1]. By 2020, worldwide consumption of aluminum products is expected to double, driven by the growth and industrialization in China, India, Russia, and Brazil according to Alcoa's 2005 Annual Report. Fuel savings of 5–7% can be realized for every 10% weight reduction by substituting aluminum for heavier steel through appropriate design [2]. Although aluminum exhibits a high strength-to-weight ratio, it can be further improved by adding reinforcements such as ceramic particles resulting in a metal matrix composite (MMC). The synthesis of cast aluminum metal matrix composite with ceramic particles reinforcement dates back to 1965

* Corresponding author.
E-mail address: arunrm@squ.edu.om (R. Arunachalam).

https://doi.org/10.1016/j.jallcom.2019.01.115
0925-8388/

when Pradeep Rohatgi discovered it [3]. Since then, many researchers have investigated the development and characterization of metal matrix composites. Over the past three decades, metal matrix composites have moved from research to commercial applications. The worldwide metal matrix composite markets as of 2004 required more than 3500 metric tons and are increasing rapidly, with an annual growth rate exceeding 6% [3]. Metal matrix composites' functional properties, including high structural efficiency, excellent wear resistance, and attractive thermal and electrical characteristics, have enabled their application in ground transportation, including auto and rail; thermal management; and the aerospace, recreational, and infrastructure industries [4]. Metal matrix composites have also been commercialized in a large number of high-performance applications [3]. Currently, metal matrix composites are used in automotive applications, including in cylinder liners, pistons, connecting rods, camshafts, tappets, brake calipers and rotors, and much more. However, the cost of these high-performance components is still high, and they are not widely used. Several approaches could be taken to reduce the cost of composites such as single-step mixing, opting for selective reinforcements, and using cheaper reinforcements [5]. A few researchers in Oman have investigated using spent catalyst waste for producing building materials, but the added value of such applications is quite low when compared to using the waste in high-performance applications such as in components for automotive industries [6,7]. Spent alumina catalyst, for example, mainly consists of alumina (71.38 wt %) so could be easily used as a reinforcement for producing aluminum metal matrix composite reinforced with alumina [6]. Around 200–500 kg of waste spent alumina catalyst is produced daily in oil refineries in Oman and pose an environmental threat [6].

Aluminium production involves very high energy consumption because its production is based on an electrolytic reduction process involving very high current [8]. It has been estimated that 20–40% of the cost of production can be accounted for by the electric power consumed during production [9]. Hence, the present approach is environmentally friendly because scrap aluminium alloy wheels were used as the matrix material for producing aluminum metal matrix composite. It has been suggested that recycling aluminum could eliminate more than 94% of the impact of global warming and fossil fuel depletion as compared to producing aluminium as a primary processes [8]. Also, transmuting waste materials into value-added composite materials to be used for different applications results in the conservation of natural resources. Economic benefits also result from the reduced cost associated with using scrap materials.

Aluminum metal matrix composites are normally produced by the established route of stir casting [10]. Although stir casting is an economical process for producing casted components, they suffer from porosity issues, which prevents their use for producing high-strength components. To overcome this issue, researchers have adopted squeeze casting. Among the metal matrix composites produced, aluminum and silicon carbide (SiC) are the most commonly investigated matrix and reinforcement materials, respectively [11,12]. Although alumina (Al_2O_3) exhibits similar properties, researchers have made relatively few attempts to develop metal matrix composites using alumina as compared to SiC. Two different metal matrix composites with the matrix-reinforcement combinations of Al6061-SiC (20 μm) and Al7075-alumina (20 μm) have been produced through stir casting [12]. The researchers recommended particle reinforced composites over fiber reinforced ones for the advantages of lower cost and better plastic forming capability as well as excellent heat and wear resistance. The Al7075- alumina composite was found to exhibit better mechanical properties than Al6061-SiC because the Al7075 matrix was found to possess better mechanical properties than the Al6061. Sajjadi and Beygi produced aluminum metal matrix composites reinforced with both micro and nano alumina particles using a bottom tapping squeeze casting facility [13]. Even though nanoparticle-reinforced metal matrix composites exhibited better mechanical properties, they had issues of agglomeration while the micron particles were uniformly dispersed in the matrix. Sajjadi and co-workers [14] investigated the microstructure and mechanical properties of aluminium - alumina micro and nanocomposites produced by squeeze casting. The researchers adopted a novel three-step mixing method that helped to improve the incorporation and uniform distribution of the nano reinforcement particles. Best mechanical properties were obtained at smaller alumina particle sizes. Yigezu and co-workers compared the performance of an aluminium alloy (AlCu4Mg2.5) reinforced with both alumina (50 μm) and SiC (50 μm) metal matrix composite produced by stir casting [15]. In terms of mechanical properties like UTS, the SiC-reinforced composite performed better than the alumina although in terms of ductility the alumina performed better. This trend can mainly be attributed to the ductile nature of the fracture in the alumina-reinforced composite, while in the SiC-reinforced composite the weak intermetallic phase Al_4C_3 formed resulted in brittle fractures. Abhishek and co-workers produced and characterized a A359/alumina metal matrix composite using an electromagnetic squeeze casting method [16]. The tensile strength of the cast composites increased with the increase in the weight fraction of alumina. Tahamtan and co-workers studied the effects of alumina reinforcing particle size (10 μm and 100 nm) in an Al-A206 matrix produced through semi-solid and liquid states [17]. The reinforcement was added in two different forms: as received alumina particles and in a pre-synthesized composite that was prepared by milling alumina with aluminium and magnesium powders. The researchers recommended adding the reinforcement in pre-synthesized forms rather than as received because the thinner interfacial reaction layer has been found to produce better tensile properties. Also, the researchers found that composites produced through a liquid state exhibited higher porosity when compared to the semi-solid state. In the liquid state during stirring, the vortex formed created turbulence which resulted in the entrapment of air resulting in higher porosity. The nanometer reinforced alumina exhibited better ultimate tensile strength (UTS) when compared to the micron-sized reinforced composite because of the fracture occurring through particle debonding. Heat treatment of 1 wt % of alumina in aluminum metal matrix composites resulted in significant improvement in mechanical properties such as hardness and compressive strength [18]. Similar to the work of Kumar and co-workers Lakshmipathy and co-workers produced metal matrix composites through stir casting but changed the matrix combinations to 7075Al/SiC and 6061Al/alumina [12,19]. The researchers mainly focused on the reciprocating wear behavior of metal matrix composites with three different reinforcement weight percentages (10, 15, and 20%) of SiC and Al_2O_3 having a size of 36 μm. An increase in the weight percentage of reinforcements resulted in higher hardness but the impact strength decreased. Maximum hardness of 50 Brinell hardness number (BHN) was recorded for the Al7075-20%SiC while the Al6061-20% alumina exhibited a lower value (37 BHN). Similarly, the wear resistance of Al7075-SiC composites was greater than that of Al6061- alumina which was mainly due to the lower volume loss because Al7075's matrix had a higher hardness. Microsized SiC and alumina have also been used together as reinforcement in aluminum metal matrix composites at different proportions to improve mechanical properties [20].

Based on the literature reviewed, all research on producing aluminum metal matrix composites by squeeze casting has used

virgin matrices and reinforcement materials. This proposed research approach is novel, therefore, because for the first time aluminum metal matrix composite was produced using scrap aluminium alloy as a matrix and spent alumina catalyst from oil refinery waste as reinforcement material. The scrap aluminium alloy (chemical formula: AlSi4Mg3Mn2Fe1) closely resembled 6000-series aluminum alloy, with the most prevalent alloying elements being silicon, magnesium, manganese, and iron. The chemical composition is illustrated in Table 1. For comparision purposes, both virgin aluminium alloy grade AlSi7Mg and alumina were used as matrix and reinforcement materials, respectively. In this research work, four different aluminum metal matrix composites were produced using a squeeze-casting process and subjected to both material and mechanical property characterizations using different techniques.

2. Materials and methods

2.1. Matrix and reinforcement materials

AlSi7Mg alloy billets and aluminium from scrap aluminium alloy were selected as matrix materials, and alumina and spent alumina catalyst were selected as reinforcing materials for developing the composites. The elemental composition of scrap aluminium alloy and spent alumina catalyst (Table 1) was determined through X-ray fluorescence (XRF) and energy dispersive X-ray spectroscopy (EDS) analysis, respectively [6]. The alumina powder (Alfa Aesar, Germany) was of high chemical purity with an average particle size of 50 μm. The spent alumina catalyst was obtained from the local petroleum refinery and had an average particle size of 150 μm.

2.2. Metal matrix composite production

Squeeze casting was utilized to produce the composites. The composition of the materials used for producing the aluminum metal matrix composites is shown in Table 2. The scrap aluminium alloy was collected from scrap stock, and dirt and grease were removed using acetone. The wheels were cut into small pieces so that they could easily pass through the opening of the crucible. The permanent hardened steel dies (50 mm in diameter and 250 mm long) were preheated to 300 °C. The temperature-controlled squeeze casting furnace was set to 750 °C. The stirrer rod and stirrer were cleaned, and a non-stick boron carbide coating was applied at room temperature and dried at 250–300 °C to withstand high temperatures and prevent erosion of the stirrer edges. The reinforcement particles were preheated in the preheater chamber at 300 °C to eliminate dampness and reduce particle clotting. The matrix materials were charged into the furnace when the crucible temperature reached around 350 °C, and the materials were further heated to 750 °C to completely melt the alloy. The stirrer rod was then switched on and gently moved into a position 30 mm above the bottom of the crucible with a stirring speed of 650 rpm. One wt. % of magnesium was added to the molten matrix to improve the wettability between the matrix and the reinforcement [21]. The preheated reinforcement particles were slowly added to the vortex formed during stirring and mixed for 10 min. The molten mixture was then transferred through a bottom tapping mechanism into the preheated pathway pipe connected to the die of the squeeze casting setup. A squeezing pressure of 200 MPa was applied immediately to the molten mixture poured into the die. The same procedure was followed for the fabrication of the remaining three samples. The procedure used for producing the aluminum metal matrix composites is shown in Scheme 1. The squeeze casting parameters for aluminum metal matrix composite fabrication are in Table 3.

Table 2
Designation and composition of composites produced by squeeze casting.

Composite	Matrix	Quantity (Kg)	Reinforcement	Quantity (g)
a	LM25	1	Al_2O_3	50
b	SAAW	1	Al_2O_3	50
c	LM25	1	SAC	50
d	SAAW	1	SAC	50

LM25 = AlSi7Mg; Al_2O_3 = Alumina; SAAW = Scrap aluminium alloy wheel; SAC = Spent alumina catalyst.

2.3. Microstructural and elemental composition characterization

The samples obtained through squeeze casting were cut to the required size and then mounted using a SimpliMet 1000 automated mounting press (Buehler, USA). An Automet 250 grinder-polisher (Buehler) was used for grinding and polishing the samples. Grinding was accomplished sequentially using 400, 600, and 1200 grit abrasive paper. Samples were then mechanically polished for five minutes with three stages of diamond suspension. Per ASTM E3-01, the finely polished samples were etched using Keller's reagent. The surface morphological analysis was carried out using an optical microscope 1000x VHZ100R (Keyence Corporation, Japan). The microstructures and elemental composition of the samples as well as the fracture and wear analyses were studied using a field emission scanning electron microscope (FESEM) model JSM-7600F (JEOL, Japan) with an attached EDS. X-ray diffraction analyses were conducted using an X'pert PRO XRD (Malvern Panalytical Ltd., UK) with Cu Kα radiation ($\lambda = 1.5418$ Å) to measure intensities of the peak and identify the different phases of the material. X-ray fluorescence analyses were conducted for scrap aluminium alloy composition analysis using an AxiosmAX (Panalytical).

2.4. Porosity and specific strength measurement

The density of the matrix and reinforcement were determined to assess the percentage of porosities present in the aluminum metal matrix composites. Density measurements were executed based on Archimedes' principle using a 10-mm wide x 30-mm long x 3-mm thick sample for all four composites. The theoretical densities of composites were calculated using the rule of mixtures [22].

Table 1
Elemental composition of Matrix and Reinforcements.

Matrix	**Al**	**Si**	**Fe**	**Cu**	**Mn**	**Mg**	**Ni**	**Pb**	**Zn**	**Ti**
LM25 (wt. %)	Balance	7.0	0.5	0.1	0.3	0.4	0.1	0.1	0.1	0.05
SAAW (wt. %)	90.15	3.81	1.16	0.21	1.62	2.74	–	0.03	0.14	0.09
Reinforcement	**Al_2O_3**	**SiO_2**	**Fe_2O_3**	**CaO**	**LOI**	**MgO**	**Na_2O**	**SO_3**	**K_2O**	**TiO_2**
Al_2O_3 (wt. %)	Balance	–	0.7	1.2	–	–	–	–	–	1.7
SAC (wt. %)	Balance	0.32	0.01	0.51	22.18	0.16	3.85	0.08	0.04	–

LM25 = AlSi7Mg; Al_2O_3 = Alumina; SAAW = Scrap aluminium alloy wheel; SAC = Spent alumina catalyst.

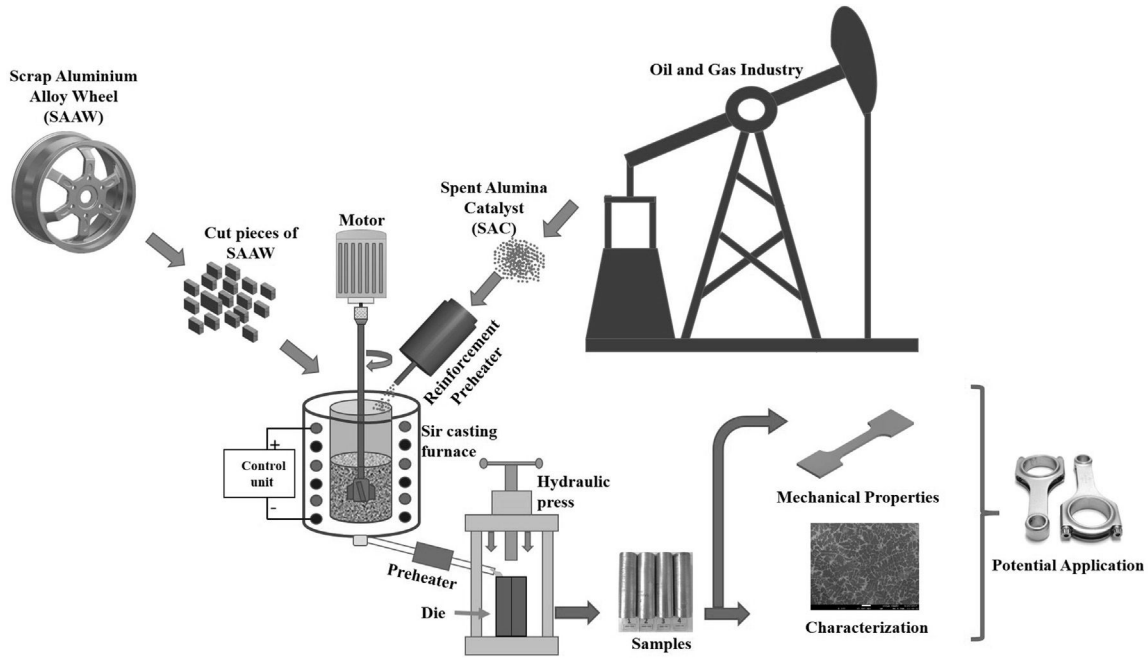

Scheme 1.

Table 3
Process parameters of squeeze casting.

S.No.	Process parameters	Values
1	Stirring temperature	750 °C
2	Stirring speed	650 RPM
3	Stirring time	10 min
4	Preheat temperature of reinforcement particles	300 °C
5	Preheat temperature of permanent die	300 °C
6	Squeeze pressure	200 MPa

The porosity in the samples were determined using Eq. (1).

$$P = 1 - \frac{\rho_{Experimental}}{\rho_{Theoratical}} \times 100 \quad (1)$$

The specific strength, or strength-to-weight ratio of the aluminum metal matrix composites, was calculated by the force-per-unit area at failure divided by its experimental density.

2.5. Mechanical and wear characterization

Samples' hardness, and compressive, tensile, and abrasive properties were evaluated. Hardness was measured with a universal hardness tester UH250 (Buehler) using the indentation technique. The Brinell and Vickers scales of hardness were used, and the average of five repeated measurements at random locations were reported. A force of 15.625 kgf was applied to determine the BHN using a 2.5 mm ball indenter gradually applied to the substrate without impact with a dwell time of six seconds. Similarly, to determine the Vickers hardness value (HV) a force of 5 kgf was applied to the substrate using a square-based diamond pyramid indenter with an included angle of 136° for a dwell time of eight seconds. Three samples were prepared from each produced aluminum metal matrix composite rod for tensile tests per ASTM B557 using a wire-cutting machine. Gripping the specimen at the two ends, the tensile load was applied. Using the stress-strain curve obtained from the machine, mechanical properties such as yield and ultimate stress of the samples were calculated. The strain rate of the tensile test was 8.33×10^{-4}/s. A compression test was carried out according to ASTM E9 using a 100 kN universal testing machine (MTS 20/MH, France). The uniaxial compression tests were performed on 20 mm high by 12 mm in diameter cylindrical samples with a crosshead speed of 1 mm/min (a strain rate of about 8.33×10^{-4}/s). Two samples for each of the four composites were then tested using a compression test. Each sample was compressed to 10 mm (half its height), and the load-stroke data were converted to stress-strain curves. An abrasion test was performed on polished substrate using a two-body TR-605 abrasion tester (Ducom Instruments, India). Four different grades of SiC emery paper (ES20, ES60, D-150, and SiC E4 600 TP4) were used with ANSI grit sizes of 20, 60, 150, and 600, respectively, with SiC E4 600 TP4 exhibiting the finest grit. A friction wheel of precisely defined dimensions held down by a known weight was moved to and fro in a straight line across the test surface. The outer diameter of the wheel was 50 mm greater than the diameter of the surface to which the emery paper was fixed. In this process, the rubbing segment of the wheel was constantly replaced by lifting the wheel off the surface and turning it to a fixed angle of 1.8° at the end of each stroke. The wheel started rubbing against the squeeze cast sample at 40 rpm with a test load of 3N. The reciprocating motion of the assembly delivered uniform abrasion to the specimen. The motor was turned off automatically after completing 200 cycles. The weight loss of the samples was measured using a weighing machine with a minimum count of 0.001 g.

3. Results and discussion

3.1. Microstructural analysis

The optical microscopic images for the four different composites at 200× magnification are shown in Fig. 1. In the pictures, grey particles are a mixture of both the reinforcement and the eutectic phase of silicon, white regions are aluminium matrix, and black regions are porous defects. All microstructures exhibited an almost non-dendrite shape at the grain boundaries because of the squeeze

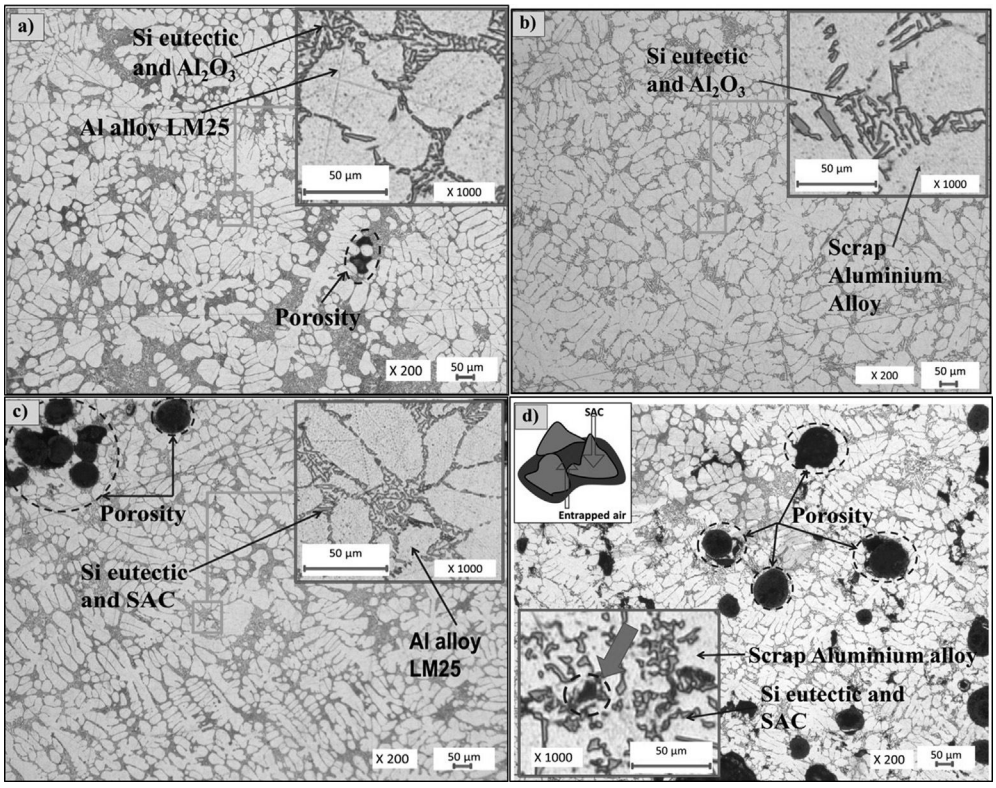

Fig. 1. Morphologies of the composites at 200× magnification: (a) AlSi7Mg (LM25) + alumina (Al_2O_3), (b) Scrap aluminium alloy wheel (SAAW) + Al_2O_3, (c) LM25 + spent alumina catalyst (SAC) and (d) SAAW + SAC.

pressure, which resulted in finer dendrites and decreased dendrite arm spacing [23]. Fig. 1(a) and (b) show that the microstructure of the composites with alumina used as a reinforcement have nearly uniform dispersion and dense structure with the exception of some of the micropores [Fig. 1(a)]. This finding was reconfirmed by the pore size and distribution (Fig. 2). Although small clusters of mixed particles from the alumina and silicon eutectic phase (explained in detail using Figs. S1 and S2 in the supporting information) can be observed in some regions [Fig. 1(a)], a uniform distribution of particles can also be observed [Fig. 1(b)]. The clustering can be attributed to the smaller size of the alumina reinforcement when compared to the spent alumina catalyst. The uniform distribution of the mixed particles at the grain boundaries may also be attributed to the smaller grain size, with an average ranging from 42 to 50 µm of both matrix materials. However, the slightly smaller size of the AlSi7Mg matrix resulted in more uniform particle distribution when compared to the scrap aluminium alloy matrix. Table 4 shows the grain sizes obtained for all four composites. The methodology for estimating the grain sizes is explained in the supporting information with the help of Fig. S3. Fig. 1(a–d) shows that the grain boundaries were occupied by the mixed particles of alumina and the Si eutectic phase [24,25]. The mixed particles were mostly positioned in the grain boundary cavities [25]. During the solidification process, alumina particles dissipated heat slowly compared with the matrix due to the lower thermal and heat diffusivity of alumina, and the liquid alloy cooled down more rapidly than the particles. In addition, the hotter particles may have transferred heat to the surrounding materials, resulting in a slower melt which may have caused delayed solidification. As a result, nucleation of the aluminium phase started in the liquid at a distance from the particles, where the temperature was lower. Therefore, the microstructure of the composites contained primary aluminium dendrites and eutectic silicon, while alumina particles were separated at the inter-dendritic regions. This event occurred more easily with the finer particles [13]. The scrap aluminium alloy + spent alumina catalyst and AlSi7Mg + spent alumina catalyst composites [Fig. 1(c) and (d)] clearly show that the addition of spent alumina catalyst to the aluminum matrix produced porosity in the samples. Spent alumina catalyst particles entrapped air [(as shown schematically in the top left corner of Fig. 1(d)],

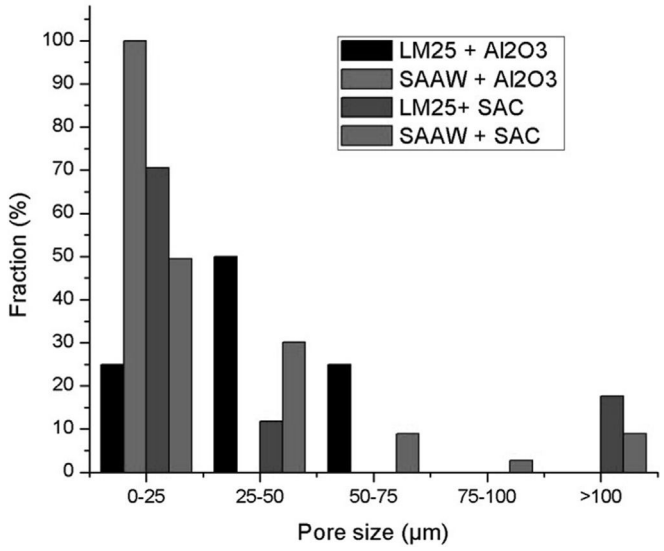

Fig. 2. Pore distribution in the composite samples (LM25: AlSi7Mg; SAAW: Scrap aluminium alloy wheel; SAC: spent alumina catalyst).

Table 4
Grain size, hardness, porosity and abrasive wear for all the four composites.

Composite	Grain size of matrix (μm)	Hardness (Brinell)	Porosity (%)	Abrasive wear (ES20)
LM25 + Al_2O_3	42.06	58.775	13.2	0.6
SAAW+ Al_2O_3	50.47	58.475	7.3	0.42
LM25 + SAC	44.41	57.675	14.3	0.68
SAAW+SAC	48.11	55.95	16.6	0.72

LM25 = AlSi7Mg; Al_2O_3 = Alumina; SAAW = Scrap aluminium alloy wheel; SAC = Spent alumina catalyst.

leading to difficulty in their integration into the melt. These agglomerated spent alumina catalyst particles entered into the melt and caused porosity [(shown as an inset in the lower left corner of Fig. 1(d)] and agglomeration of spent alumina catalyst particles in the composite [26]. Similar results were observed in an earlier publication where some porosity was found to be usual in aluminum metal matrix composites [27]. This finding was attributed to the longer particle feeding time, which increased the time of contact with air.

Fig. 2 shows the pore size distribution for the four composites based on analysis of the optical micrograph images (Fig. 1) [28]. Fig. S4 in the supporting information describes the procedure adopted to find the pore size and distribution. Fig. 2 shows that micropores (0–25 μm) constituted more than 80% of the pores in the composites, and less than 20% of the pores were over 100 μm in size. The larger size pores (>100 μm) were only found in composites reinforced with spent alumina catalyst (Table S2 in the supporting information shows the size ranges and number of pores). The air entrapment mechanism detailed in Fig. 1(d) explains why the pore sizes as well as the number of pores are higher in the spent alumina catalyst reinforced composites. The fractured surfaces of the composites reinforced with spent alumina catalyst (Fig. 10) indicate poor wettability with the matrix, resulting in pore nucleation of the surfaces and larger pore sizes as well as higher porosity in the matrix reinforced with spent alumina catalyst [14]. In the case of the scrap aluminium alloy + alumina composite, 100% of the pores are in the 0–25 μm range and it is only one pore (Table S2). Similarly, AlSi7Mg + alumina also exhibited smaller pore sizes and fewer pores (Table S2). The pore distribution data was consistent with the porosity volume percentage reported in Fig. 5A.

Fig. 3 shows the field emission scanning electron microscope images of the four composite samples at 300× magnification. The distribution of reinforcement in the matrix of the composite is visible in the micrograph. The light and dark grey particles are the reinforcement and matrix, respectively. The microstructure of both matrix materials (AlSi7Mg and scrap aluminium alloy) consisted of primary α phase aluminum dendrites and eutectic silicon [13]. The alumina particles were separated at the inter-dendritic regions and in the eutectic silicon so appeared as a mixture [29]. This mixture is evident in the zoomed area shown as the inset of Fig. 3(a), which shows that the eutectic silicon phase morphology is mostly a mixture of slightly acicular spherical structures and some blunted, needle-like shapes as well. This type of morphology, and especially the spherical and blunted needle shapes, reduces the stress concentration, enhancing mechanical properties as can be seen from the ultimate tensile strength values discussed later [30,31]. The smaller size as well as the higher alumina content as compared to the spent alumina catalyst provided more nucleation sites for the eutectic silicon phase. Moreover, the higher-content silicon in the AlSi7Mg alloy resulted in a denser mixture in the eutectic silicon phase and the reinforcement [Fig. 3(a) and (c)].

The scanning electron micrographs [Fig. 3(a) and (b)] show that the alumina reinforcement particles mixed with the eutectic silicon appeared well dispersed in the matrix, although some small clusters remained in the microstructure of AlSi7Mg + alumina [Fig. 3(a)]. This finding can mainly be attributed to the smaller size of the alumina reinforcement, which tends to aggregate due to high surface energy [32]. Fig. 3(c) and (d) depicting AlSi7Mg + spent alumina catalyst and scrap aluminium alloy + spent alumina catalyst composites also show a uniform distribution of reinforcements throughout the sample but with micropores. Fig. 3(d)'s inset shows micropores. These porosities are mainly due to the larger size of the spent alumina catalyst particles (150 μm) which act as nucleation sites for the pores. Also, as explained earlier, the spent alumina catalyst particles entrap air which leads to micropores around the reinforcement particles [Fig. 1(d)].

X-ray diffraction analysis was carried out for phase identification and to measure peak intensity. Fig. 4 shows the X-ray diffraction analyses of the four samples. All four patterns show that the highest intensity peaks were for the aluminium matrix (38.66°) and the alumina reinforcement (44.42°). The other alloying elements present in elevated amounts, such as the silicon, magnesium, and iron present in the matrix material, also appeared as low intensity peaks. The aluminum peaks were in the (1 1 1) and (2 2 0) planes while, for alumina, the peaks were in the (2 0 2) plane. Similarly, the planes for silicon, silicon dioxide (SiO_2), magnesium, and iron were silicon (1 1 1), silicon (2 2 0), SiO_2 (3 1 1), magnesium (2 1 1) and iron (2 1 1), respectively. These peaks were identified using Xpert HighScore software (Malvern Panalytical) and peaks were matched with the International Centre for Diffraction Data (ICDD) database. The peaks were high enough to prove that the materials were polycrystalline in nature and that the particles were arranged in cubic order. The structure of atoms was arranged in a hexagonal closed packed system and packed highly efficiently. This finding may be attributed to the pressure applied during squeeze casting [33].

The composite using AlSi7Mg grade as a matrix material had significant silicon content which was indicated by the relatively higher intensity peaks [Fig. 4(a) and (c)]. Although the silicon content was higher in the AlSi7Mg grade, the absence of new phases with silicon indicated no adverse reactions. Similarly, the slightly higher intensity peaks of magnesium and iron in the composites based on the scrap aluminium alloy did not indicate any adverse reactions with either the alumina [Fig. 4(b)] or spent alumina catalyst [Fig. 4(d)]. The inactivity of iron in the matrix may be attributed to the levels below the critical iron level, so no iron-containing intermetallic phases were formed [34]. The X-ray diffraction pattern of the AlSi7Mg and alumina combination [Fig. 4(a)] showed higher intensity peaks for alumina because it has higher alumina content as compared to the composite produced using spent alumina catalyst as reinforcement (~70% alumina). Similar higher intensity peaks for alumina were also obtained [Fig. 4(b)] because of the higher alumina content. Similarly, the X-ray diffraction patterns [Fig. 4(a) and (b)] in which alumina was used as a reinforcement did not reveal any new phase formation with the aluminum in the matrix and so was quite stable. This stability may be attributed to the compatability of the alumina with the aluminium matrix. A similar trend was also noted [Fig. 4(c) and (d)] in samples where spent alumina catalyst was used as the reinforcement. The patterns indicate the absence of high levels of

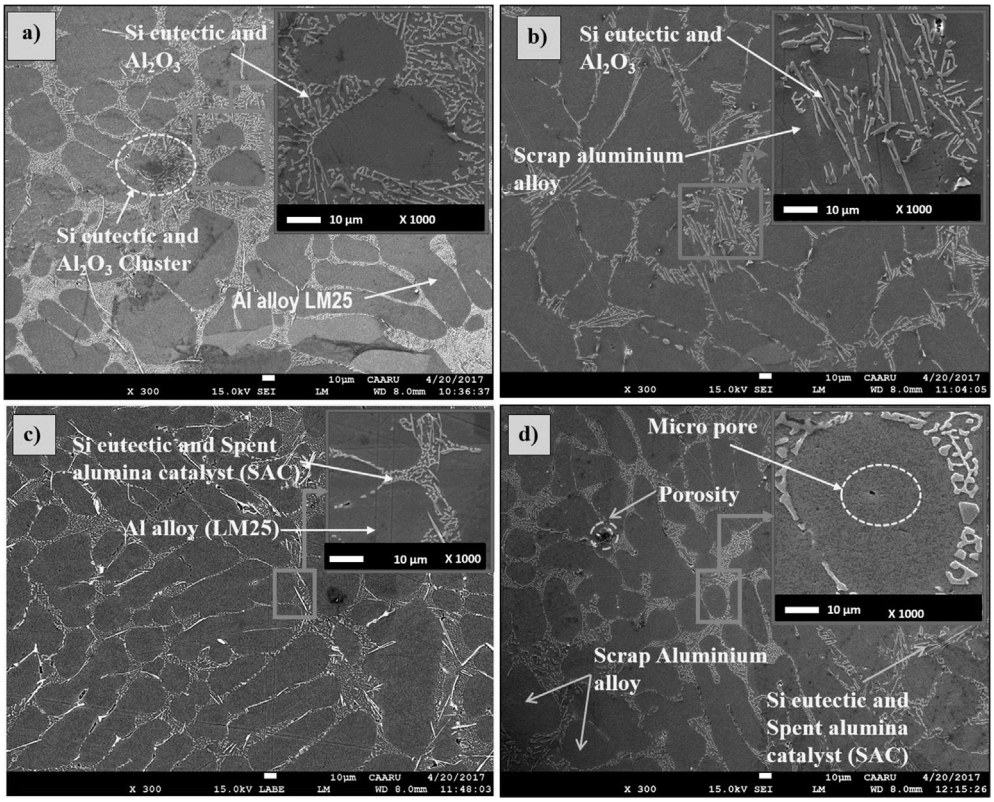

Fig. 3. SEM images of composites at 300× magnification: (a) AlSi7Mg (LM25) + alumina (Al_2O_3), (b) Scrap aluminium alloy wheel (SAAW) + Al_2O_3, (c) LM25 + spent alumina catalyst (SAC) and (d) SAAW + SAC.

new phase formation. The composite with alumina reinforcement produced higher peak intensity [Fig. 4(a) and (b)] when compared to the spent alumina catalyst phase [Fig. 4(c) and (d)]. The higher alumina content was a main cause of the improved mechanical strength of the composite, and the trend matched the tensile and compressive properties discussed later.

3.2. Porosity and specific strength

Porosity affects the properties of materials based on pore size, distribution of reinforcements, and other characteristics. It is almost impossible to completely avoid porosity in aluminium castings because shrinkage results from volume contraction that occurs during solidification as well as gas evolution. This phenomenon is due to a decrease in the gas solubility of solid metal as compared to the liquid form [35]. In addition to the porosity formed due to shrinkage and gas evolution, adding reinforcement particles also increases the sites for pore formation; thus, composites exhibit higher porosity than pure matrix materials. Generally, if porosity is low, fewer empty spaces are found in the composite material, and it will be stronger. In the current study, the calculated porosity results matched the obtained optical micrograph. The scrap aluminium alloy + alumina composite sample showed much lower porosity while samples with spent alumina catalyst reinforcement exhibited higher porosity (Fig. 5). The higher silicon content in the AlSi7Mg matrix resulted in more nucleation sites around the reinforcement, so the frequency of micropores was higher when compared to the scrap aluminium alloy, which had a lower silicon content. In the squeeze casting process, the higher pressure used during solidification aided in proper filling of the die, reducing casting defects and especially those related to porosity. This phenomenon is illustrated in the experimental density obtained and illustrated in Fig. 5(A). The squeeze casting process was quite successful in achieving experimental density close to the theoretical density [36]. The higher porosity in the case of spent alumina catalyst may be attributed to the nature of its application. Spent alumina catalyst is mainly used to reduce emissions of volatile organic compounds (VOCs) to the atmosphere [37]. These volatile compounds present in the spent alumina catalyst contribute to the higher porosity. The mechanism of the gas entrapment was discussed earlier [Fig. 1 (d)].

Fig. 5(B) shows that the strength-to-weight ratio of the AlSi7Mg + alumina aluminum metal matrix composite was highest followed by the scrap aluminium alloy + alumina aluminum metal matrix composite. Although the AlSi7Mg + alumina composite exhibited higher porosity than the scrap aluminium alloy + alumina, it showed the highest specific strength, which was due to a higher concentration of the acicular shaped eutectic silicon phase mixture that acted as a barrier for dislocation movement in the matrix [30,38].

3.3. Hardness

Fig. 6 shows the hardness values on both the Brinell and Vicker scales for all four composites. The Brinell hardness values correlated well with the ultimate tensile strength values discussed in the next section. The two tests were conducted by indentation where the indenter was pressed into the sample under specific standard force. However, a steel ball indenter was used in the Bricknell test while a square-base diamond pyramid indenter was used in the Vickers test. The Vicker hardness values were highly influenced by the location of the indentation because of the instrument's sharp tip, possibly explaining the reason for the Vicker hardness values not being well correlated with the tensile strength of the composites. This feature of instrumentation is the reason for the

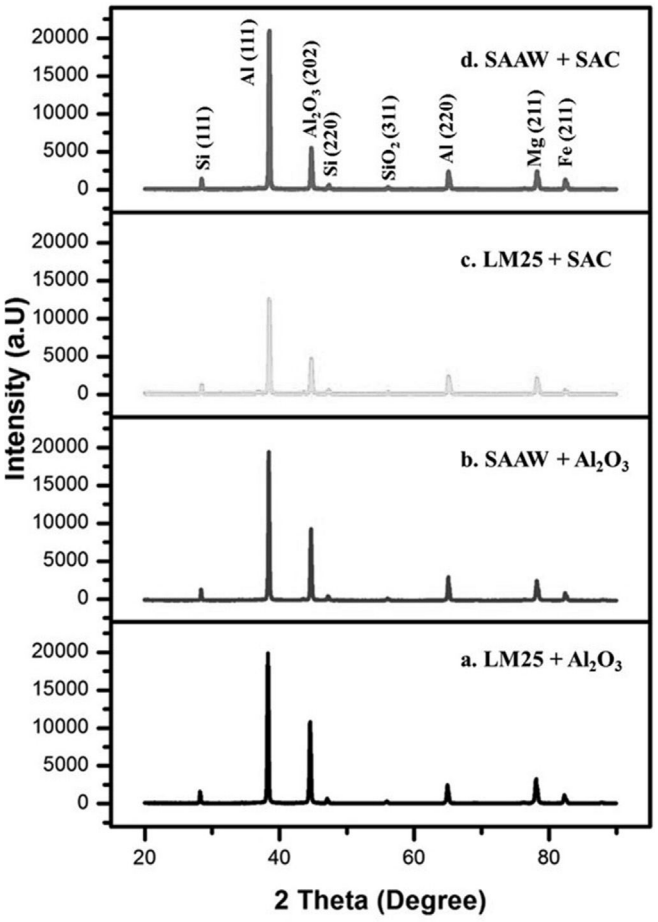

Fig. 4. XRD patterns of the composites: (a) AlSi7Mg (LM25) + alumina (Al_2O_3), (b) Scrap aluminium alloy wheel (SAAW) + Al_2O_3, (c) LM25 + spent alumina catalyst (SAC) and (d) SAAW + SAC.

observed scattering in the Vicker hardness values; thus, the Brinell hardness test is recommended for bulk composites with micron-sized reinforcement particles.

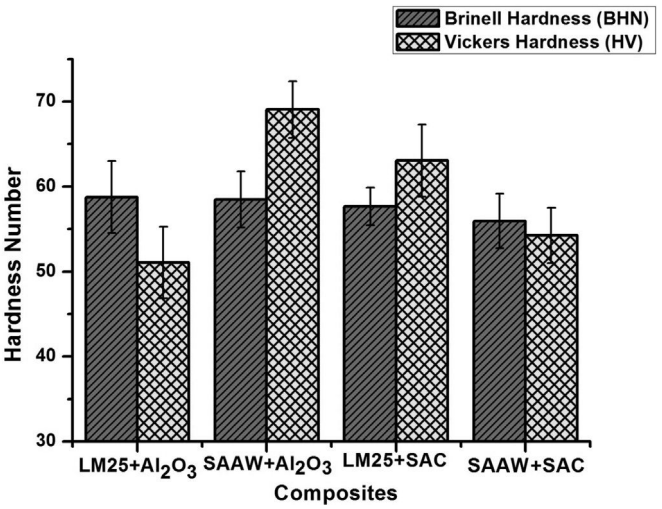

Fig. 6. Brinell and Vickers hardness values for the produced composites (LM25: AlSi7Mg; SAAW: Scrap aluminium alloy wheel; SAC: spent alumina catalyst).

The BHN values obtained for the four composites did not vary to a great degree (Table 4). However, a trend can be inferred based on the values obtained for the four composites. The highest hardness was found in the AlSi7Mg + alumina composite (58.8 BHN) followed very closely by the scrap aluminium alloy + alumina composite (58.5 BHN). The hardness for the AlSi7Mg + spent alumina catalyst composite was 57.7 BHN followed by 56 BHN for the scrap aluminium alloy + spent alumina catalyst composite. The higher BHNs for the alumina-based reinforcements were mainly due to the smaller size of the alumina particles as compared to the spent alumina catalyst. It can also be inferred that the smaller grain size of the AlSi7Mg matrix contributed to the higher hardness values obtained (Table 4). With the decrease in grain size, the hardness of the material increased [39]. The porosity also influenced the hardness, and the data show that the scrap aluminium alloy + spent alumina catalyst composite had the highest porosity and the lowest hardness, because the porosity sites acted as microsites for easy dislocation movement [Table 4].

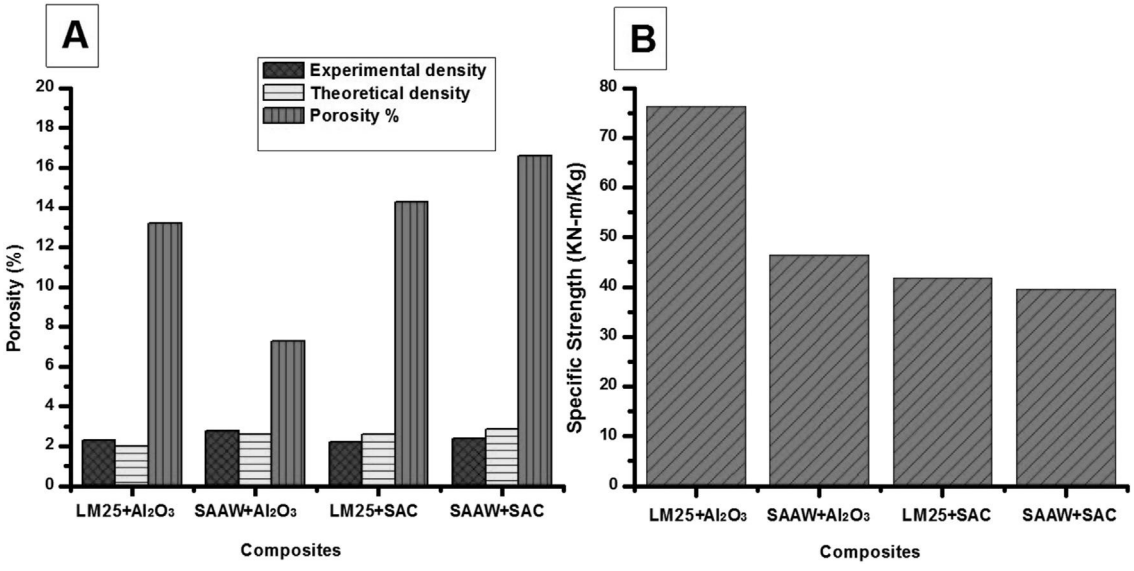

Fig. 5. (A) Percentage of porosity and (B) specific strength of the composites; (LM25: AlSi7Mg; SAAW: Scrap aluminium alloy wheel; SAC: spent alumina catalyst).

Table 5 shows a comparison of the hardness and porosity values for composites produced by different researchers primarily using alumina as the main reinforcement by the stir/squeeze casting processes. Because the matrix materials, size, types of reinforcement and percentages used are quite different for the composites reported, each finding is unique; therefore, it is quite difficult to compare previous findings with those of the present work. However, in general the hardness as well as the porosity values obtained in this work are comparable with those in the literature. The hardness values in brackets were converted from different scales to the BHN scale for comparison purposes using a hardness conversion chart for aluminium [40]. This conversion, however, must be regarded as only an estimate for research purposes. Table 5 shows that the particle size (ranging from 10 to 70 μm) and porosity (ranging from 2.9 to 11%) influenced the hardness significantly. The smaller particle sizes provided more interfacial area, which served as the nucleation site for grain formation. When the particle size is smaller, the spacing between the particles is reduced. The smaller particles then exert more constraint on grain growth during cooling and more restriction on plastic flow during deformation, which can also contribute to an increase in hardness and strength [41]. Higher porosity always results in lower hardness because the porosity sites act as zones for easy dislocation movement. It can be inferred from the data in Table 5 that the squeeze casting process can greatly reduce porosity due to the pressure applied during solidification, helping micropores coalesce in the casting.

3.4. Tensile and compressive strength

The tensile stress-strain curves of the four different types of aluminum metal matrix composites are shown in Fig. 7. Tensile properties such as yield strength (σ_y), ultimate tensile strength (UTS), elongation to fracture (ε_f), and fracture stress (σ_f) were extracted from these stress-strain curves [Table 6]. The σ_y of AlSi7Mg + alumina was 53 MPa. The ultimate tensile strength of AlSi7Mg + alumina was 172 MPa with a ε_f of 4.6% and a σ_F of 171 MPa AlSi7Mg + alumina displayed the predominance of tensile properties as compared to other combinations of samples. In the case of scrap aluminium alloy + alumina, the values for σ_y, ultimate tensile strength, ε_f, and σ_f were 37.3 MPa, 125 MPa, 2.7% and 125 MPa, respectively. The sample made with spent alumina catalyst as reinforcement showed very low tensile strength because of higher porosity (Figs. 1 and 3) as well as the calculated percentage of porosity. The ultimate tensile strength of the AlSi7Mg + spent alumina catalyst and scrap aluminium alloy + spent alumina catalyst composites were measured as 93 MPa and 82 MPa, respectively. AlSi7Mg + alumina was found to be relatively more ductile than the other specimens, followed by scrap aluminium alloy + alumina. This finding could be due to the lower porosity and more uniform distribution of the alumina reinforcement in the matrix.

From the information in Table 6, it can be inferred that the reinforcement particle size greatly influenced the ultimate tensile strength. An increase of 85% and 52.4% in the ultimate tensile strength was achieved when alumina was used as a reinforcement in AlSi7Mg and the scrap aluminium alloy matrix, respectively, instead of the spent alumina catalyst. The smaller size of the alumina as well as the higher content (the spent alumina catalyst had a lower alumina content) provided more sites for nucleation of the silicon eutectic phase, and this mixture of particles in the grain boundaries acted as an obstacle, restricting the motion of dislocations in the matrix [14]. In addition, the uniform distribution of the particles in the mixture as confirmed by the optical and scanning electron microscopic images helped in transferring the applied tensile load to the uniformly distributed strong mixture of alumina and eutectic silicon phase particles [14]. When comparing the composite produced using the AlSi7Mg and the scrap aluminium alloy as a matrix with alumina as reinforcement, the AlSi7Mg showed an increase of 37.6% in the ultimate tensile strength value over the scrap aluminium alloy. Again, this finding is mainly because of the higher silicon content in the AlSi7Mg which resulted in a higher mixture of the alumina and the eutectic silicon phase as well as the smaller grain size of the matrix (Table 4). Only a small increase (13.4%) in the ultimate tensile strength was observed when AlSi7Mg was used as a matrix and was compared to the scrap aluminium alloy matrix (both matrices were reinforced with spent alumina catalyst). As explained earlier in this work, the smaller grain size of the AlSi7Mg resulted in the higher ultimate tensile strength value. The higher porosity as well as the poor bonding (discussed in the following fracture analysis of the composites) between the reinforcement particle mixture and the matrix resulted in lower ultimate tensile strength values when spent alumina catalyst was used as a reinforcement.

The compression test was carried out on the samples to determine compression properties and identify fracture patterns. Fig. 8 depicts the stress-strain curves acquired from compression tests. Table 6 also shows the compression properties such as yield strength (σ_{yc}), ultimate compressive strength (UCS), and fracture stress (σ_{fc}) extracted from these stress-strain curves. The AlSi7Mg + alumina composite exhibited the highest σ_{fc} (336 MPa) at a deformation up to eight mm from the original length, with an ultimate compressive strength of 346 MPa. For the scrap aluminium alloy + alumina composite, the σ_{fc} occurred at 248 MPa at a deformation up to eight mm, and the ultimate compressive strength of the aluminum metal matrix composite was 312 MPa. These findings suggest that scrap aluminium alloy + alumina had a slightly lower load-bearing capacity than other composites tested perhaps due to the higher hardening rate in the AlSi7Mg alloy matrix. A similar phenomenon was seen in the compressive response of the AlSi7Mg + alumina composite as well as the smaller grain size of the AlSi7Mg (Table 4). The σ_{fc} of the AlSi7Mg + spent alumina catalyst composite was 221 MPa at a

Table 5
Comparisons of hardness and porosity of various composites primarily reinforced with alumina.

S. No.	Composites	Wt./Vol. fraction (%)	Casting Method (Applied pressure)	Particle size	Porosity (%)	Hardness	References
1	A356 (Al-Si7Mg)/Al_2O_3	3	Stir	20 μm	2.9	77 BHN	[14]
2	SAAW/Al_2O_3	5	Squeeze (200 Mpa)	50 μm	7	57 BHN	**[Our work]**
3	Pure Al/Al_2O_3	1	Stir	40 μm	8	52 HV (47 BHN)	[24]
4	AA2024 (AlCu4Mg1)/Al_2O_3	10	Stir	32 μm	5	105 BHN	[27]
5	AA2024 (AlCu4Mg1)/Al_2O_3	5	Stir	50 μm	8.4	82 HV (72 BHN)	[15]
6	AA6061 (AlMg1SiCu)/Al_2O_3	20	Stir	36 μm	–	38 BHN	[19]
7	LM25 (Al-Si7Mg)/2% Al_2O_3/3% B_4C	5	Stir	70 μm	–	52 BHN	[43]
8	AA6061 (AlMg1SiCu)/3% Al_2O_3/2% B_4C	5	Stir	50 μm	–	64 HRB (104 BHN)	[20]
9	A356 (Al-Si7Mg)/Al_2O_3	1	Stir	30 μm	–	63 BHN	[18]

BHN = Brinell hardness number; HV = Vickers hardness value; Al_2O_3 = Alumina.

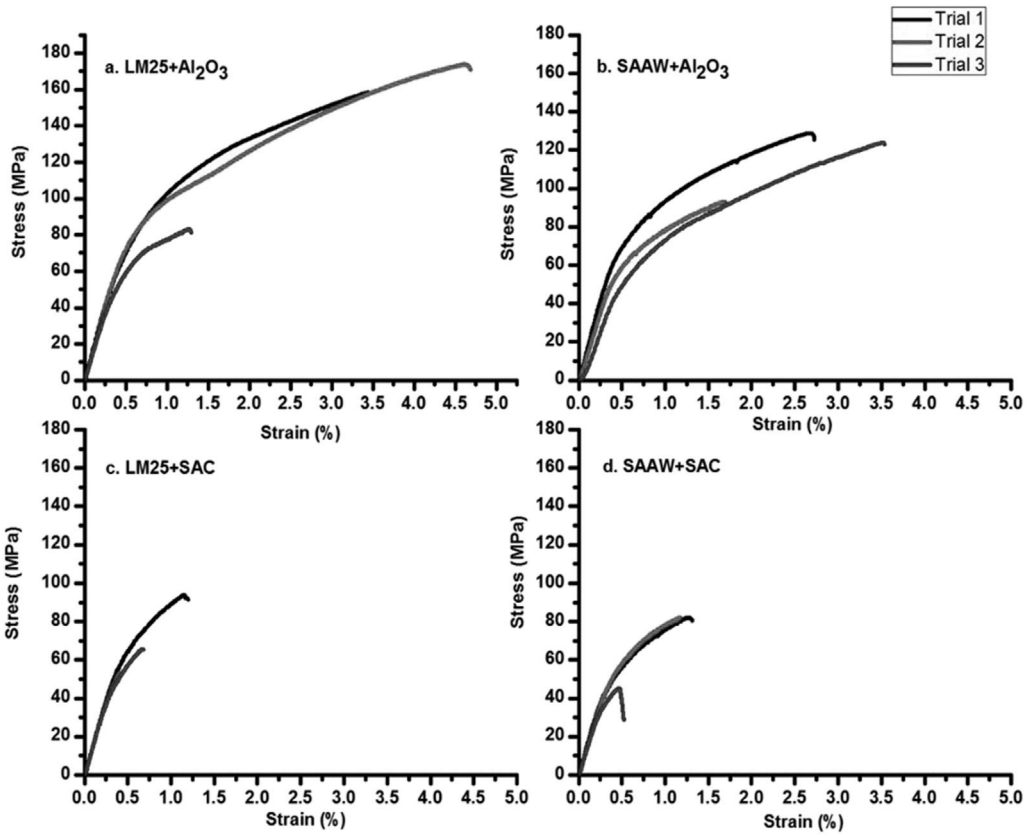

Fig. 7. Tensile stress strain curves for the produced composites: (a) AlSi7Mg (LM25) + alumina (Al_2O_3), (b) Scrap aluminium alloy wheel (SAAW) + Al_2O_3, (c) LM25 + spent alumina catalyst (SAC) and (d) SAAW + SAC.

Table 6
Room temperature tensile and compressive properties of the four composites.

Composite	σ_y (MPa)	UTS (MPa)	ε_f (%)	σ_f (MPa)	$\sigma_{y(c)}$ (MPa)	UCS (MPa)	$\sigma_{f(c)}$ (MPa)
LM25 + Al2O3	52.74	172	4.6	171.1	217	346	336
SAAW+ Al2O3	37.33	125	2.7	125	178	312	248
LM25 + SAC	29	93	1.17	91.4	135	234	221
SAAW+SAC	21	82	0.25	94.5	115	274	265

LM25 = AlSi7Mg; Al_2O_3 = Alumina; SAAW = Scrap aluminium alloy wheel; SAC = Spent alumina catalyst.

deformation of five mm from the original length. In contrast, scrap aluminium alloy + spent alumina catalyst's ultimate compressive strength was found to be 265 MPa at a deformation of six mm from the original length, indicating a sharp decrease in the load-bearing capacity of the aluminum metal matrix composites reinforced with spent alumina catalyst. The ultimate compressive strength of AlSi7Mg + spent alumina catalyst and scrap aluminium alloy + spent alumina catalyst were 234 MPa and 274 MPa, respectively, which correlated with the porosity observed in micrographs as well as the porosity percentage. Thus, it can be concluded that the effect of reinforcement type (especially the size) on both tensile and compressive strengths was significant. For the same matrix alloy (AlSi7Mg), alumina reinforced composites resulted in a 48% increase in the ultimate compressive strength as compared to those reinforced with spent alumina catalysts. This finding confirms the significant effect of the alumina mixed with the silicon eutectic phase in strengthening the composites by acting as a barrier for crack propagation. During the compression tests, all samples bulged, or deformed, in a barrel shape, and they continued to do so until fracturing (Fig. 8 inset). In all cases, the sample did not detach itself along the diagonal planes after fracture. The presence of a friction constraint between contacting flat sample ends generated a non-uniform plastic flow in the compressed samples. Such non-uniformity of the flow and accompanying materials weakened the composites and created shear deformation in the diagonal plane. Small increases in ultimate compressive strength for the scrap aluminium alloy matrix reinforced with alumina (14% higher than the same matrix reinforced with spent alumina catalyst) were obtained. Similarly, an 11% increase in ultimate compressive strength for the alumina reinforced in the AlSi7Mg matrix was obtained as compared to the scrap aluminium alloy reinforced with the same alumina. The higher alumina concentration (as compared to the spent alumina catalyst) as well as the higher silicon content in the AlSi7Mg matrix (as compared to the scrap aluminium alloy) helped create more nucleation sites for the mixture of the alumina and eutectic silicon which accounted for the higher value of ultimate compressive strength in the above two composites.

The yield and ultimate strength estimated from the stress-strain curves of the aluminum metal matrix composite samples for both

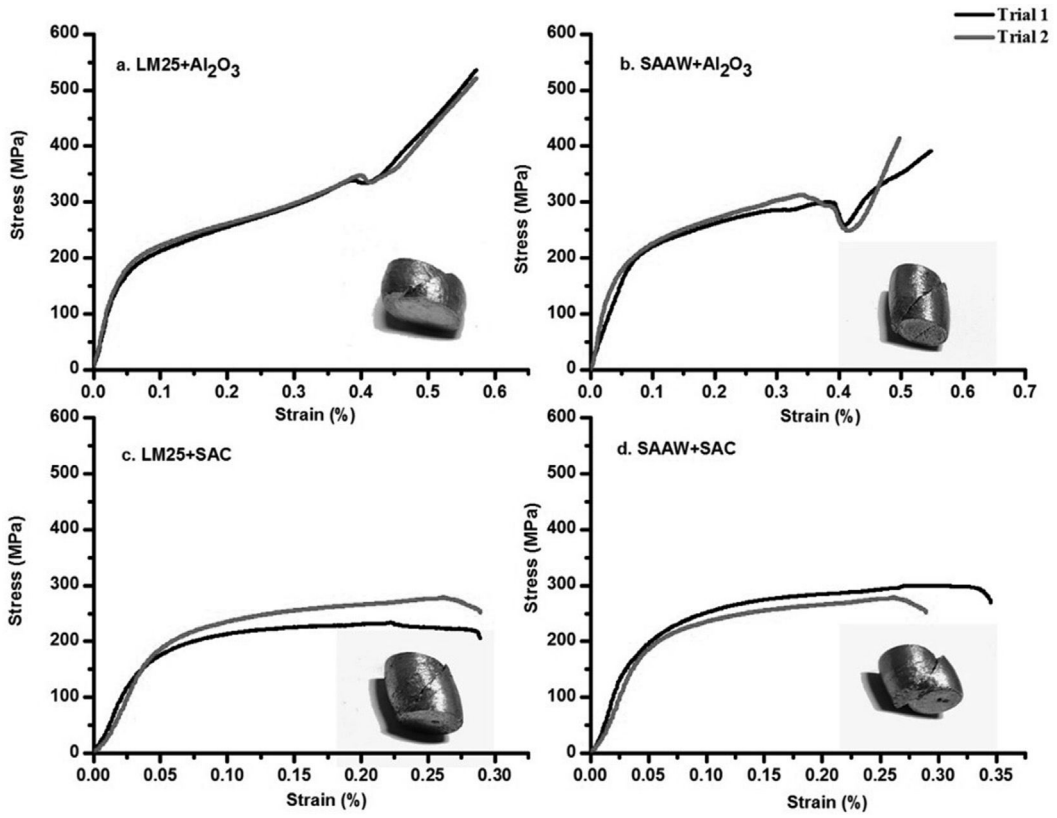

Fig. 8. Compression stress strain curves with inset image of fracture indication for the produced composites: (a) AlSi7Mg (LM25) + alumina (Al_2O_3), (b) Scrap aluminium alloy wheel (SAAW) + Al_2O_3, (c) LM25 + spent alumina catalyst (SAC) and (d) SAAW + SAC.

tensile and compressive tests are shown in Fig. 9. Based on the tensile and compressive strength, the AlSi7Mg + alumina composite showed superior properties followed by the scrap aluminium alloy + alumina composite. The higher strength of the AlSi7Mg + alumina composite can be attributed to the higher silicon weight percentage (7 wt %) in the matrix [38]. As explained in the section on morphological analysis, the mixture of acicular eutectic silicon and reinforcement at the grain boundaries enhanced the mechanical properties. The intergranular distribution at the grain boundaries provided better mechanical properties and prevented failure along grain boundaries. The smaller grain size of the AlSi7Mg matrix, especially with the alumina reinforcement, also contributed to the enhanced mechanical properties. The smaller size of the alumina reinforcement provided more nucleation sites for the eutectic silicon phase. The trends shown in Fig. 9 suggest an exception in the ultimate compressive strength value in the case of the scrap aluminium alloy (17% higher than the AlSi7Mg matrix) reinforced with the same spent alumina catalyst. This trend can be explained by the higher levels of porosity in the composites with scrap aluminium alloy as a matrix, which acted as zones for

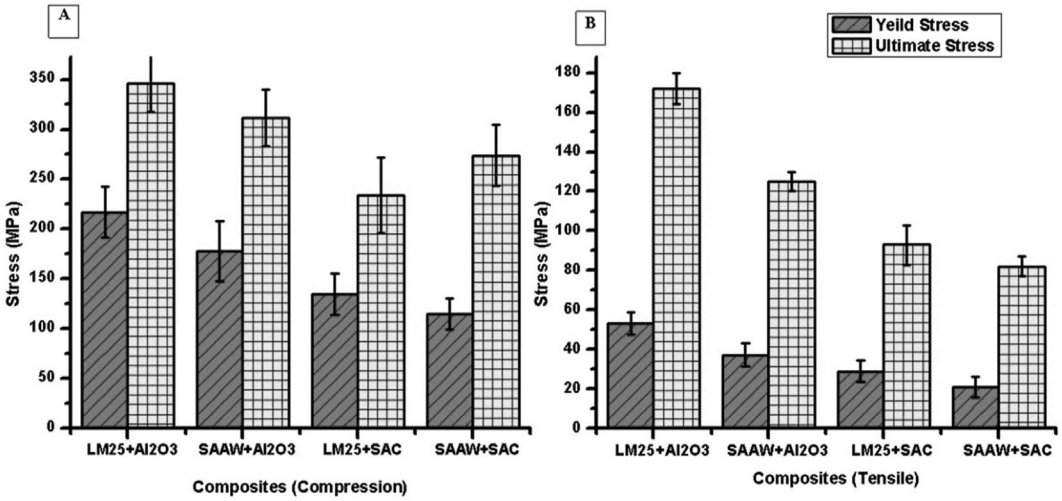

Fig. 9. Yield and ultimate strengths of the composites (LM25: AlSi7Mg; SAAW: Scrap aluminium alloy wheel; SAC: spent alumina catalyst): (A) Compression and (B) Tensile.

absorbing the compressive force; thus, they showed a higher ultimate compressive strength. During tensile loading, the higher porosity acted as a site for the crack propagation, so a slightly lower ultimate tensile strength was obtained as compared to that of the AlSi7Mg matrix.

All tensile samples were fractured within the gauge length. Fig. 10 shows the scanning electron microscopic images of the fracture surfaces of all four composites. It is obvious from the fracture surface morphology that the samples have failed predominantly because of the brittle mode of fracture, although very little ductility could be observed based on the presence of a few dimples in the matrix region of the morphology. This finding was also supported by the tensile performance depicted in Fig. 7. The fracture surface was not completely perpendicular to the direction of the applied stress, which is an indication that the material was not purely brittle but had some ductility due to the aluminum matrix material's property. The stress-strain curves illustrated in Fig. 7 corroborate this behavior. The relatively more dimpled, fractured appearance of the AlSi7Mg matrix confirms that the AlSi7Mg matrix was more ductile compared to the scrap aluminium alloy, and this finding is again in line with the stress-strain curves. In all the composites reinforced with alumina as well as spent alumina catalyst, voids appeared due to debonding of the reinforcement particles from the matrix. The inset image in Fig. 10 (b) shows a typical void created by debonding of the reinforcement. The voids' dimensions matched the average reinforcement particle size of 50 μm and 150 μm for alumina and spent alumina catalyst, respectively. Poor wetting and interfacial bonding with the matrix resulted in these types of voids [42]. In the case of composites reinforced with spent alumina catalyst, some of the spent alumina catalyst particles were still attached loosely in their position [inset image in Fig. 10 (c)], and this finding was more obvious in the case of the scrap aluminium alloy + spent alumina catalyst metal matrix composite. The larger size of the spent alumina catalyst particles resulted in a weak interfacial bonding between the matrix and the reinforcement so particle fracturing did not occur [17]. Fig. 10(c) and (d) also show that the number of pores was higher, particularly for the scrap aluminium alloy + spent alumina catalyst composite in which large-sized pores are visible. The AlSi7Mg + alumina composite also had a deep pore as illustrated in the inset image of Fig. 10 (a). This finding was consistent with the porosity measurements illustrated in Fig. 5 (A), where the scrap aluminium alloy + spent alumina catalyst composite showed the highest porosity percentage, and it was confirmed by a large number of pores in the microstructure images [Fig. 1(c) and (d)].

The tensile and compressive strengths of aluminum metal matrix composites with alumina as reinforcement which earlier researchers produced using the squeeze casting process are shown in Fig. 11 [17,18,20,43–46]. The aluminum metal matrix composites produced using scrap aluminium alloy as a matrix exhibited a similar ultimate tensile strength value as other aluminum metal matrix composites, while a slightly better compressive strength was observed when compared to other aluminum metal matrix composites reported in the literature. This finding suggests that the scrap aluminium alloy matrix is a good candidate as a matrix material for aluminum metal matrix composite production.

3.5. Abrasion wear

Fig. 12 shows the weight loss of the aluminum metal matrix composite samples when subjected to an abrasive wear test. The scrap aluminium alloy + alumina composite experienced the lowest weight loss when compared to other composite samples subjected to the abrasive sheets. SiC E4 600 TP4 had the finest grit

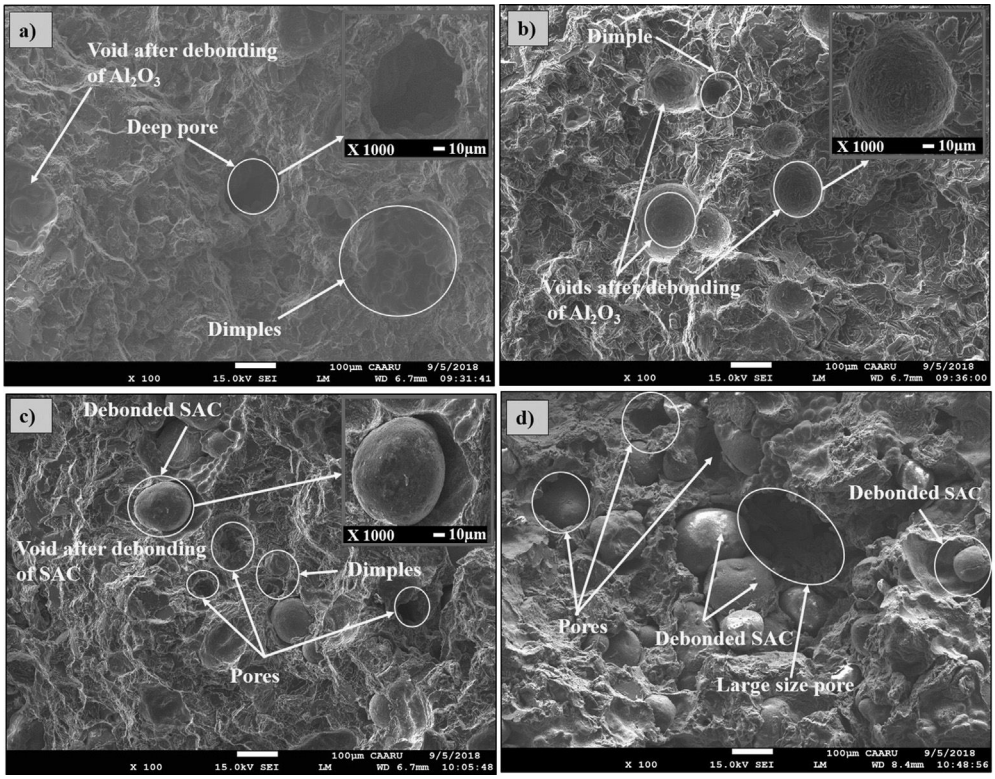

Fig. 10. Fracture surface morphology of tensile test samples (a) AlSi7Mg (LM25) + alumina (Al_2O_3), (b) Scrap aluminium alloy wheel (SAAW) + Al_2O_3, (c) LM25 + spent alumina catalyst (SAC) and (d) SAAW + SAC.

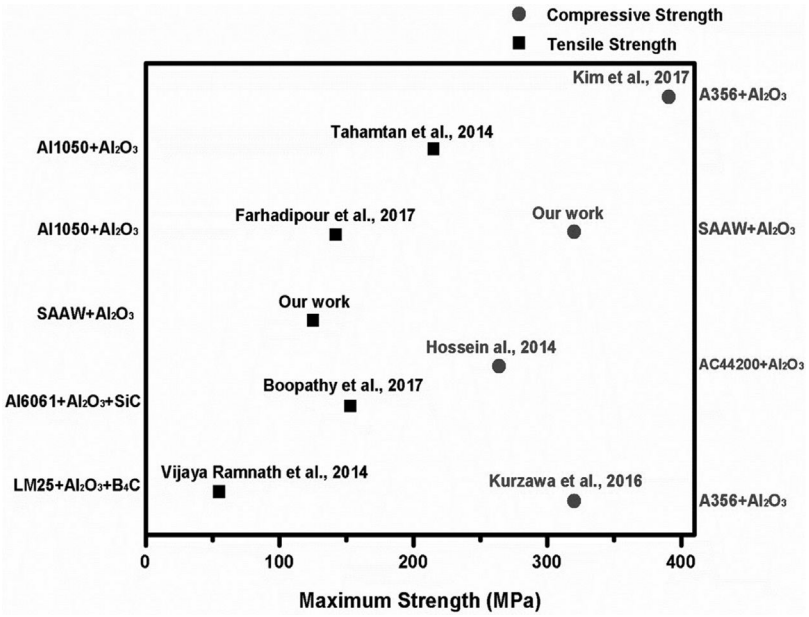

Fig. 11. Comparison of compressive and tensile strengths of various composites primarily reinforced with alumina.

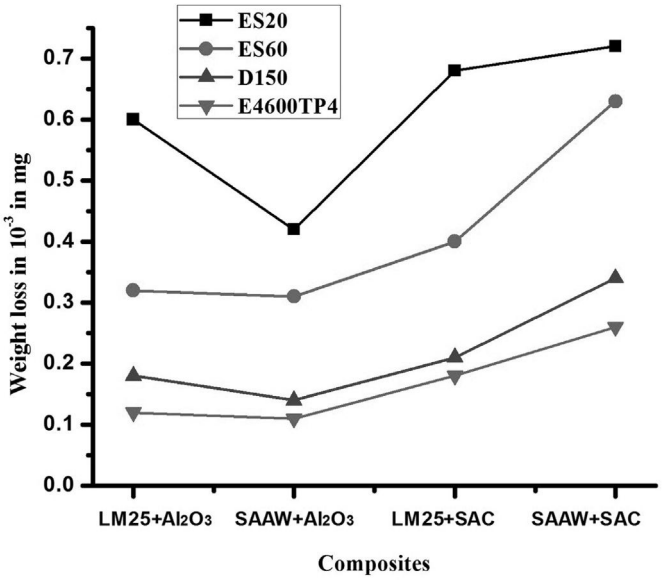

Fig. 12. Weight loss of the composites subjected to abrasion test (LM25: AlSi7Mg; SAAW: Scrap aluminium alloy wheel; SAC: spent alumina catalyst).

and produced a weight loss of 0.01 g for the scrap aluminium alloy + alumina composite. The next finest grit sheet produced weight loss of 0.015 g for the same composite. ES60 and ES20 produced weight losses of 0.038 g and 0.041 g, respectively. It was noted that the increase of roughness on the mating parts increased the wear rate of the samples, and the materials' hardness was directly proportional to the materials' wear resistance. This finding was confirmed by Brinell hardness values for the four composites (Table 4). The better wear resistance of the scrap aluminium alloy + alumina sample can be attributed to its greater hardness as well as the uniform distribution of reinforcements, refined grain structure, and lower porosity as compared to other samples.

Fig. 13 shows the scanning electron microscopic images of the wear morphology of the scrap aluminium alloy + alumina composite that exhibited the minimum wear rate for the ES20 abrasive sheet (coarsest grade) among the four composite samples during abrasion. Fig. 13 (A) clearly shows diminished wear tracks and grooves. The absence of localized delamination on the worn surface as well as dislodged particles indicate that no reinforcement particles were detached. Grooves are the characteristic feature of abrasive wear, but there was an absence of prominent scratching tracks and groves parallel to the abrasion. Fig. 13 (B) shows very few surface deformations, including sub-surface cracks, even with the very coarse abrasive loaded wheel. Surface deformation is a centre for crack nucleation, with propagation leading to greater wear rates [47]. The repeated sliding action of the abrasive wheel on the composites induces fatigue stresses, causing sub-surface cracks [48]. The plastically displaced matrix material can be observed in the magnified image shown as an inset in Fig. 13 (B), but the matrix was not affected much.

4. Conclusions

A novel approach was successfully utilized for the first time to produce aluminum metal matrix composites for potential industrial applications. The produced aluminum metal matrix composite is not only economical but also environmentally friendly because it uses scrap or waste materials. The key findings are summarized as follows:

- The micrograph analysis showed that the scrap aluminium alloy + alumina composite had a uniform distribution of reinforcements and the lowest porosity among the four composites. The composite porosity observed in the micrographs correlated with the percentage of porosity measured using Archimedes' principle.
- X-ray diffraction analyses confirmed no significant phase formation in the aluminum metal matrix composites regardless of whether scrap aluminium alloy or spent alumina catalyst was used.
- Among the four composites, the highest hardness (58.8 BHN) was obtained for the AlSi7Mg + alumina composite followed

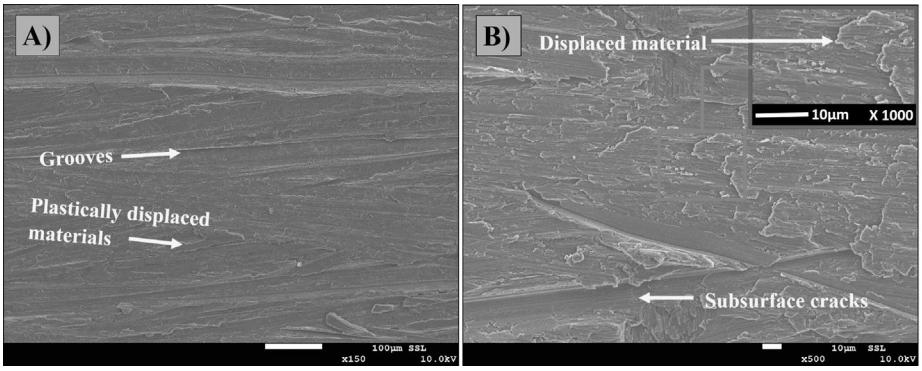

Fig. 13. SEM images of the wear morphology of the scrap aluminium alloy wheel (SAAW) + alumina composite: (A) X150 (B) X500.

very closely by the scrap aluminium alloy + alumina composite (58.5 BHN).

- The highest ultimate tensile and compressive strength values were obtained for the AlSi7Mg + alumina composite (172 MPa and 346 MPa, respectively). The second highest values were obtained by the scrap aluminium alloy + alumina composite (125 MPa and 312 MPa, respectively).
- The significantly higher ultimate tensile and compressive strength values in the composites reinforced with alumina can be mainly attributed to the formation of the reinforcement mixed with the eutectic silicon phase exhibiting a morphology that was a slightly acicular, predominantly spherical structure with some blunted, needle-like shapes.
- The addition of the spent alumina catalyst as reinforcement in both of the matrix materials resulted in higher porosity due to the air entrapment mechanism; therefore, the materials exhibited lower mechanical properties.
- The fracture surface of the tensile test samples of all the composites failed predominantly through the brittle mode of fracture, although a limited ductile mode could also be observed.
- The abrasion wear test results showed that the scrap aluminium alloy + alumina composite possessed the highest wear resistance among the four prepared aluminum metal matrix composite samples. The wear morphology of the scrap aluminium alloy + alumina composite exhibited diminished wear tracks and grooves even for the coarsest grade of abrasive sheet among the four composite samples.

In the present investigations, optimal mechanical properties were obtained for scrap aluminium alloy + alumina, composite; thus, it is recommended for potential industrial applications. Using scrap aluminium alloy as a matrix material is a viable approach for producing low-cost, high-performance aluminum metal matrix composites. Scrap aluminium alloy can be utilized as an alternative low-cost matrix material instead of virgin AlSi7Mg. Future studies could focus on optimizing the process parameters of squeeze casting and exploring nano particles as reinforcement that could further enhance the mechanical properties for high-end applications.

Declaration of interest

None.

Acknowledgement

The authors thank Sultan Qaboos University (SQU), Sultanate of Oman and the United Arab Emirates University (UAEU), Al-Ain, United Arab Emirates for providing research support through collaborative research project (SQU: CL/SQU-UAEU/17/04 and UAEU: 31N270). The Central Analytical and Applied Research Unit (CAARU) in SQU is acknowledged for providing support through analytical facilities such as SEM, XRF and XRD reported in this manuscript. The Surface Science Lab (SSL) in SQU is also acknowledged for extending SEM for the wear analysis.

Appendix A. Supplementary data

Supplementary data to this article can be found online at https://doi.org/10.1016/j.jallcom.2019.01.115.

References

[1] N. Gangil, A.N. Siddiquee, S. Maheshwari, Aluminium based in-situ composite fabrication through friction stir processing: a review, J. Alloys Compd. 715 (2017) 91–104, https://doi.org/10.1016/j.jallcom.2017.04.309.
[2] J. Cui, H.J. Roven, Recycling of automotive aluminum, Trans. Nonferrous Met. Soc. China (English Ed. 20 (2010) 2057–2063, https://doi.org/10.1016/S1003-6326(09)60417-9.
[3] K.G. Gupta, Nikhil, Satyanarayana, The solidification processing of metal-matrix composites, in: Rohatgi Symp. JOM, 2006, pp. 92–94.
[4] D.B. Miracle, Metal matrix composites - from science to technological significance, Compos. Sci. Technol. 65 (2005) 2526–2540, https://doi.org/10.1016/j.compscitech.2005.05.027.
[5] P.K. Rohatgi, D. Weiss, N. Gupta, Applications of fly ash in synthesizing low-cost MMCs for automotive and other applications, JOM 58 (2006) 71–76, https://doi.org/10.1007/s11837-006-0232-4.
[6] H. Al-dhamri, K. Melghit, Use of alumina spent catalyst and RFCC wastes from petroleum refinery to substitute bauxite in the preparation of Portland clinker, J. Hazard. Mater. 179 (2010) 852–859, https://doi.org/10.1016/j.jhazmat.2010.03.083.
[7] A. Siham Said Rabeea Al-Siyabi, Shahjahan and Jesil, Reuse of spent catalyst from sohar refinery as an additive in cement tiles 2 (2013) 464–468.
[8] Y. Zhang, M. Sun, J. Hong, X. Han, J. He, W. Shi, X. Li, Environmental footprint of aluminum production in China, J. Clean. Prod. 133 (2016) 1242–1251, https://doi.org/10.1016/j.jclepro.2016.04.137.
[9] The Aluminum Association, 2017, 2017, p. 1. http://www.aluminum.org/industries/production/primary-production. (Accessed 18 March 2018).
[10] A. Kumar, K. Pal, S. Mula, Simultaneous improvement of mechanical strength, ductility and corrosion resistance of stir cast Al7075-2% SiC micro- and nanocomposites by friction stir processing, J. Manuf. Process. 30 (2017) 1–13, https://doi.org/10.1016/j.jmapro.2017.09.005.
[11] G. Sozhamannan, S. Balasivanandha, V.S.K. Venkatachalapathy, Effect of process parameter of stir casting on metal matrix composites, Int. J. Surf. Eng. Mater. Adv. Technol. 2 (2012) 11–15, https://doi.org/10.4236/jsemat.2012.21002.
[12] G. Veeresh Kumar, C. Rao, N. Selvaraj, M. Bhagyashekar, Studies on Al6061-SiC and Al7075-Al 2 O 3 metal matrix composites, J. Miner. Mater. Char. Eng. 9 (2010) 43–55, https://doi.org/10.4236/jmmce.2010.91004.
[13] S.A. Sajjadi, H.R. Ezatpour, H. Beygi, Microstructure and mechanical properties of Al-Al2O3 micro and nano composites fabricated by stir casting, Mater. Sci. Eng. A 528 (2011) 8765–8771, https://doi.org/10.1016/j.msea.2011.08.052.
[14] S.A. Sajjadi, H.R. Ezatpour, M. Torabi Parizi, Comparison of microstructure and mechanical properties of A356 aluminum alloy/Al2O3 composites fabricated by stir and compo-casting processes, Mater. Des. 34 (2012) 106–111, https://doi.org/10.1016/j.matdes.2011.07.037.

[15] B.S. Yigezu, M.M. Mahapatra, P.K. Jha, Influence of reinforcement type on microstructure , hardness , and tensile properties of an aluminum alloy metal matrix composite, J. Miner. Mater. Char. Eng. 1 (2013) 124–130, https://doi.org/10.4236/jmmce.2013.14022.
[16] S. Kumar, Abhishek Kumar, Shyam Lal, Fabrication and characterization of A359/Al2O3 metal matrix composite using electromagnetic stir casting method, J. Mater. Res. Technol. (2013) 250–254, https://doi.org/10.1016/j.jmrt.2013.03.015.
[17] S. Tahamtan, M. Emamy, A. Halvaee, Effects of reinforcing particle size and interface bonding strength on tensile properties and fracture behavior of Al-A206/alumina micro/nanocomposites, J. Compos. Mater. 48 (2014) 3331–3346, https://doi.org/10.1177/0021998313509860.
[18] M. Hossein-Zadeh, O. Mirzaee, P. Saidi, Structural and mechanical characterization of Al-based composite reinforced with heat treated Al2O3 particles, Mater. Des. 54 (2014) 245–250, https://doi.org/10.1016/j.matdes.2013.08.036.
[19] J. Lakshmipathy, B. Kulendran, Reciprocating wear behavior of 7075Al/SiC in comparison with 6061Al/Al 2O3 composites, Int. J. Refract. Met. Hard Mater. 46 (2014) 137–144, https://doi.org/10.1016/j.ijrmhm.2014.06.007.
[20] S. Boopathy, K. Manikanda Prasath, Structure–property correlation of Al–SiC–Al2O3 composites: influence of processing temperatures, Trans. Indian Inst. Met. 70 (2017) 2441–2447, https://doi.org/10.1007/s12666-017-1105-y.
[21] K. Kanayo, M. Oluwatosin, A.A. Awe, Microstructure , mechanical and fracture properties of groundnut shell ash and silicon carbide dispersion strengthened aluminium matrix composites, J. King Saud Univ. Eng. Sci. (2016), https://doi.org/10.1016/j.jksues.2016.01.001.
[22] S.P. Dwivedi, S. Sharma, R.K. Mishra, Microstructure and mechanical behavior of A356/SiC/Fly-ash hybrid composites produced by electromagnetic stir casting, J. Braz. Soc. Mech. Sci. Eng. 37 (2015) 57–67, https://doi.org/10.1007/s40430-014-0138-y.
[23] M. singh, R.S. Rana, R. Purohit, Krishnkant sahu, development and analysis of Al-matrix nano composites fabricated by ultrasonic assisted squeeze casting process, Mater. Today Proc. 2 (2015) 3697–3703, https://doi.org/10.1016/j.matpr.2015.07.146.
[24] M. Hossein-zadeh, O. Mirzaee, P. Saidi, Production of micro-nano Al-Al 2O3 composite and investigation production of micro-nano Al-Al 2 o 3 composite, in: 15th Int. Metall. Mater. Congr., 2010, pp. 1–6.
[25] J. Lakshmipathy, B. Kulendran, Materials Reciprocating wear behavior of 7075Al/SiC in comparison with, RMHM, Int. J. Refractory Met. Hard 46 (2014) 137–144, https://doi.org/10.1016/j.ijrmhm.2014.06.007.
[26] S. Tahamtan, A. Halvaee, M. Emamy, M.S. Zabihi, Materia ls and Design Fabrication of Al/A206 – Al 2 O 3 nano/micro composite by combining ball milling and stir casting technology, Mater. Des. 49 (2013) 347–359, https://doi.org/10.1016/j.matdes.2013.01.032.
[27] M. Kok, Production and mechanical properties of Al2O3 particle-reinforced 2024 aluminium alloy composites, J. Mater. Process. Technol. 161 (2005) 381–387, https://doi.org/10.1016/j.jmatprotec.2004.07.068.
[28] B. Zhao, T. Yu, W. Ding, X. Li, Effects of pore structure and distribution on strength of porous Cu-Sn-Ti alumina composites, Chin. J. Aeronaut. 30 (2017) 2004–2015, https://doi.org/10.1016/j.cja.2017.08.008.
[29] R. Muraliraja, R. Arunachalam, I. Al-fori, M. Al-maharbi, S. Piya, Development of alumina reinforced aluminum metal matrix composite with enhanced compressive strength through squeeze casting process, Proc. Inst. Mech. E Part L J. Mater. Des. Appl. 0 (2018) 1–8, https://doi.org/10.1177/1464420718809516.
[30] V. Sharma, S. Kumar, O.P. Pandey, Correlation of reinforced ceramicparticle's nature and size with microstructure and wear behavior of Al-Si alloy composite, Adv. Mater. Res. 585 (2012) 564–568, https://doi.org/10.4028/www.scientific.net/AMR.585.564.
[31] M. Mansoor, I. Salam, A. Tauqir, Effect of micro-structural modifier on the morphology of silicon rich secondary phase and strain hardening behavior of eutectic Al-Si alloy, IOP Conf. Ser. Mater. Sci. Eng. 146 (2016), https://doi.org/10.1088/1757-899X/146/1/012033.
[32] M. Hosseinzadeh, O. Mirzaee, H. Mohammadian-Semnani, Evaluation of microstructural and mechanical properties of A356 composite strengthened by nanocrystalline V8C7-Al2O3 particles synthesized through mechanically activated sintering 782 (2018) 879–885, https://doi.org/10.1016/j.jallcom.2018.12.150.
[33] H.Z. Fang, R.X. Li, R.R. Chen, B.Y. Yu, Y.D. Qu, S.W. Xun, R. De Li, Microstructure and mechanical properties of Al-6Zn-2.5Mg-1.8Cu alloy prepared by squeeze casting and solid hot extrusion, Trans. Nonferrous Met. Soc. China (English Ed. 25 (2015) 2130–2136, https://doi.org/10.1016/S1003-6326(15)63824-9.
[34] J.A. Taylor, Iron-containing intermetallic phases in Al-Si based casting alloys, Proc. Mater. Sci. 1 (2012) 19–33, https://doi.org/10.1016/j.mspro.2012.06.004.
[35] H.R. Ammar, A.M. Samuel, F.H. Samuel, Effect of casting imperfections on the fatigue life of 319-F and A356-T6 Al-Si casting alloys, Mater. Sci. Eng. A 473 (2008) 65–75, https://doi.org/10.1016/j.msea.2007.03.112.
[36] C. Kannan, R. Ramanujam, Comparative Study on the Mechanical and Microstructural Characterisation of AA 7075 Nano and Hybrid Nano-composites Produced by Stir and Squeeze Casting, Cairo University, 2017, https://doi.org/10.1016/j.jare.2017.02.005.
[37] Chemical Processing, 2017, in: https://www.chemicalprocessing.com.
[38] J. Clarke, A.D. Sarkar, Wear characteristics of as-cast binary aluminium-silicon alloys, Wear 54 (1979) 7–16, https://doi.org/10.1016/0043-1648(79)90044-9.
[39] G. Liu, N. Zhao, C. Shi, E. Liu, F. He, L. Ma, Q. Li, A In-situ synthesis of graphene decorated with nickel nanoparticles for fabricating reinforced 6061Al matrix composites, Mater. Sci. Eng. 699 (2017) 185–193, https://doi.org/10.1016/j.msea.2017.05.084.
[40] Spectro, Hardness Conversion Chart for Aluminium Products, 2017, http://www.spectro.in/Hardness-Conversion-Chart-for-Aluminium.html. (Accessed 27 December 2018).
[41] M. Dhanashekar, V.S. Senthil Kumar, Squeeze casting of aluminium metal matrix composites - an overview, Proc. Eng. 97 (2014) 412–420, https://doi.org/10.1016/j.proeng.2014.12.265.
[42] P. Van Trinh, J. Lee, P.N. Minh, D.D. Phuong, S.H. Hong, Effect of oxidation of SiC particles on mechanical properties and wear behavior of SiCp/Al6061 composites, J. Alloys Compd. 769 (2018) 282–292, https://doi.org/10.1016/j.jallcom.2018.07.355.
[43] B. Vijaya Ramnath, C. Elanchezhian, M. Jaivignesh, S. Rajesh, C. Parswajinan, A. Siddique Ahmed Ghias, Evaluation of mechanical properties of aluminium alloy-alumina-boron carbide metal matrix composites, Mater. Des. 58 (2014) 332–338, https://doi.org/10.1016/j.matdes.2014.01.068.
[44] M. Davanageri, S. Narendranath, R. Kadoli, Dry sliding wear behavior of super duplex stainless steel AISI 2507: a statistical approach, Arch. Foundry Eng. 16 (2016) 47–56, https://doi.org/10.1515/afe.
[45] P. Farhadipour, M. Sedighi, M. Heydari Vini, Using warm accumulative roll bonding method to produce Al-Al 2 O 3 metal matrix composite, Proc. Inst. Mech. Eng. Part B J. Eng. Manuf. 231 (2017) 889–896, https://doi.org/10.1177/0954405417703421.
[46] C.S. Kim, K. Cho, M.H. Manjili, M. Nezafati, Mechanical performance of particulate-reinforced Al metal-matrix composites (MMCs) and Al metal-matrix nano-composites (MMNCs), J. Mater. Sci. 52 (2017) 13319–13349, https://doi.org/10.1007/s10853-017-1378-x.
[47] N. Saheb, T. Laoui, A.R. Daud, M. Harun, S. Radiman, R. Yahaya, Influence of Ti addition on wear properties of Al – Si eutectic alloys, Wear 249 (2001) 656–662, https://doi.org/10.1016/S0043-1648(01)00687-1.
[48] N. Saheb, T. Laoui, A.R. Daud, R. Yahaya, S. Radiman, Microstructure and hardness behaviours of Ti-containing Al-Si alloys Microstructure and hardness behaviours of Ti-containing, Philos. Mag. A 82 (2002) 803–814, https://doi.org/10.1080/01418610208243203.